



Rigorous prediction of Raman intensity from multi-layer films

NATHAN VAN VELSON,^{1,3} HAMIDREZA ZOBEIRI,² AND XINWEI WANG^{2,4} 

¹Research and Development Department, Advanced Cooling Technologies, Inc., 1046 New Holland Ave., Lancaster, PA 17601-5688, USA

²271 Applied Science Complex II, Department of Mechanical Engineering, Iowa State University, 1915 Scholl Rd, Ames, IA 50011-2103, USA

³nathan.vanvelson@1-act.com

⁴xwang3@iastate.edu

Abstract: In the Raman probing of multilayer thin film materials, the intensity of the measured Raman scattered light will be impacted by the thickness of the thin film layers. The Raman signal intensity will vary non-monotonically with thickness due to interference from the multiple reflections of both the incident laser light and the Raman scattered light of thin film interfaces. Here, a method for calculating the Raman signal intensity from a multilayer thin film system based on the transfer matrix method with a rigorous treatment of the Raman signal generation (discontinuity) is presented. This calculation methodology is valid for any thin film stack with an arbitrary number of layers with arbitrary thicknesses. This approach is applied to several thin film material systems, including silicon-on-sapphire thin films, graphene on Si with a SiO₂ capping layer, and multilayer MoS₂ with the presence of a gap between layers and substrate. Different applications where this method can be used in the Raman probing of thin film material properties are discussed.

© 2020 Optical Society of America under the terms of the [OSA Open Access Publishing Agreement](#)

1. Introduction

Thin film materials are integral to many aspects of modern life, with silicon integrated circuits and thin film transistors being the most prominent [1–2], but also solar cells, light emitting diodes, thermoelectric devices, and various sensors [3–5]. Additionally, next generation two-dimensional atomic layer materials such as graphene and transition metal dichalcogenides are becoming ever more prevalent in research. The now familiar material graphene, which is a two-dimensional hexagonal array of carbon atoms, has attracted significant interest due to its unique electrical, thermal, and mechanical properties [6–7]. Similarly, transition metal dichalcogenides (TMDs) of the form MX₂ (where M = Mo, W; X = S, Se, or Te), which are semiconductive in nature, have generated significant research interest due to their potential for applications in a wide range of electronic and optical devices [8–9]. Furthermore, these 2D materials can be stacked into multi-layer structures in which the layers are weakly bonded by van der Waals forces [10]. These so-called van der Waals (VDW) heterostructures also have numerous potential applications [11].

Raman spectroscopy has been commonly used to characterize the structure of thin film materials outlined above. Raman spectroscopy is an optical spectroscopy technique used in analytical chemistry that is based on the inelastic scattering of incident light by optical phonons in materials [12]. When a photon is incident upon a molecule, it sends the molecule into a higher energy virtual state before being reemitted. In most cases the scattered light is at the same wavelength as the incident light. A small number of photons however are scattered at a different wavelength as the molecule settles into a different vibrational state; this is known as Raman scattering. The wavelength of the scattered light depends on the molecular structure of the material, and can therefore be used as a fingerprint for identifying different materials [13].

Raman spectroscopy is therefore useful for probing the structure of materials [14]. It is also observed that temperature can impact the Raman signal in terms of intensity, frequency (Raman shift) and linewidth. This enables non-contact and non-destructive temperature measurements to be made of Raman active materials [15]. Our lab has developed multiple methods for materials thermal characterization using Raman spectroscopy-based techniques [16–18].

Previous research has shown that in the Raman probing of supported films, the intensity of the Raman signal is non-monotonic as a function of film thickness [19–21]. This has been shown to be due to interference of both the incident light as well as the Raman signal from multiple reflections at the interfaces with the substrate and the environment. Previous studies have calculated the Raman signal intensity vs. thickness for one- or two-layer films on a semi-infinite substrate from the Fresnel equations and calculations of optical path length [19–21]. However, a general solution for predicting the Raman signal intensity as a function of thickness for films with an arbitrary number of layers has not yet been reported. Additionally, previous calculations of the Raman intensity calculation of one- or two-layer films do not rigorously treat the Raman signal generation within the film. In the work by Wang *et al.* [20], the forward and backward Raman scattering in the Raman active film is treated at the same phase, which will lead to errors in the Raman signal evaluation. In the work by Yoon *et al.* [21], the non-continuity of the Raman signal in the Raman active layer (due to Raman signal generation) is not considered.

In this paper, we report on the rigorous calculation of the Raman signal intensity from a Raman-active layer in a multi-layer film stack, properly taking into account the Raman signal generation and propagation within the film, using the transfer matrix method (TMM). The calculation is adaptable to any film with an arbitrary number of layers, where any layer in the film can be Raman-active. The backward and forward Raman signal generations are considered separately, which can be treated to be coherent or with specific phase lag. Additionally, when calculating the Raman signal as a function of thickness, the layer with varying thickness and the Raman-active layer need not be the same. In the following section, we present the derivation of the Raman intensity calculation. Application of the calculation approach is then demonstrated for several material systems: epitaxial silicon-on-sapphire (SOS), multi-layer graphene over silicon dioxide on a silicon substrate, and multi-layer MoS₂ on Si with a spacing between the layers and the substrate. Potential applications for utilizing these calculations are also discussed.

2. Theory

2.1. Laser propagation in the multi-layer system

For a multi-layer thin film subject to an incident plane wave, the transfer matrix method (TMM) can be applied to determine the overall transmission and reflection coefficients, as well as the electric field amplitude at any location in the film stack [22–24]. Consider the multi-layer film in Fig. 1, the components of the electric field amplitude in the positive and negative directions at the front and back surfaces of the film stack are related by the transfer matrix S .

$$\begin{pmatrix} E_0^+ \\ E_0^- \end{pmatrix} = S \begin{pmatrix} E_{m+1}^+ \\ E_{m+1}^- \end{pmatrix}, \quad (1)$$

where

$$S = \begin{pmatrix} S_{11} & S_{12} \\ S_{21} & S_{22} \end{pmatrix} = \left(\prod_{n=1}^m I_{(n-1)n} L_n \right) \cdot I_{m(m+1)}. \quad (2)$$

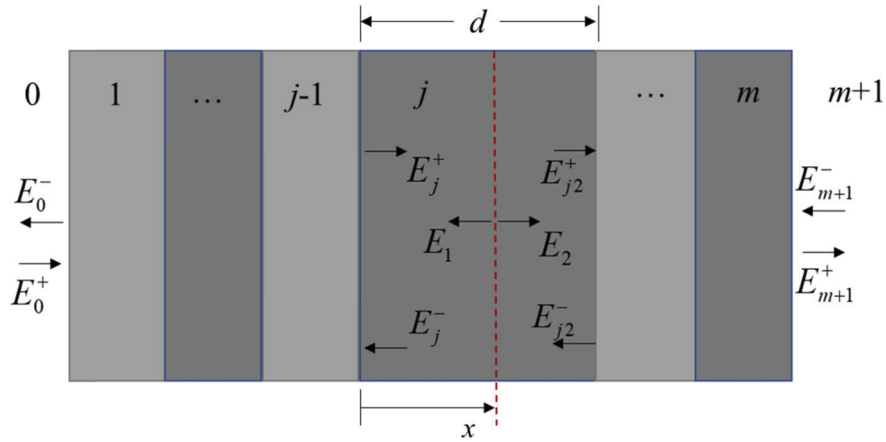


Fig. 1. General multilayer thin film structure having m layers between ambient (layer 0) and semi-infinite substrate (layer $m+1$). Each layer j has a thickness d_j and a unique complex index of refraction. The electric field at any point is comprised of a component propagating in the positive direction and a component propagating in the negative direction. If layer j is Raman active, the Raman signal emanating from location x within has a backward propagating component E_1 and a forward propagating component E_2 .

Here I_{jk} is the interface transfer matrix for the interface between medium j and medium k . It is defined from the interface reflectance coefficient r_{jk} and transmittance coefficient t_{jk} as

$$I_{jk} = \begin{pmatrix} 1/t_{jk} & r_{jk}/t_{jk} \\ r_{jk}/t_{jk} & 1/t_{jk} \end{pmatrix}. \quad (3)$$

For a plane wave with normal incidence, which is an adequate approximation for a back-scattering Raman setup, the reflectance and transmittance coefficients are the same for both s- and p-polarized light and simplify to

$$r_{jk} = \frac{\tilde{n}_j - \tilde{n}_k}{\tilde{n}_j + \tilde{n}_k}, \quad t_{jk} = \frac{2\tilde{n}_j}{\tilde{n}_j + \tilde{n}_k} \quad (4)$$

Here, \tilde{n}_j is the complex index of refraction $\tilde{n}_j = n_j + ik_j$ for layer j . L_j is the propagation matrix for layer j , which defines the absorption and phase shift that occurs in layer j , and is defined as

$$L_j = \begin{pmatrix} e^{-i\beta_j d_j} & 0 \\ 0 & e^{i\beta_j d_j} \end{pmatrix}, \quad (5)$$

where $\beta_j = (2\pi/\lambda)\tilde{n}_j$.

The matrix transfer method can be used to determine the electric field amplitude at any position in a multilayer film stack [25]. First, we recognize that for layer j , the total transfer matrix can be expressed as $S = U_j L_j D_j$ where the upstream and downstream transfer matrices are respectively

$$U_j = \left(\prod_{n=1}^{j-1} I_{(n-1)n} L_n \right) \cdot I_{(j-1)j} \quad (6)$$

and

$$D_j = \left(\prod_{n=j+1}^m I_{(n-1)n} L_n \right) \cdot I_{m(m+1)}. \quad (7)$$

From these definitions, it can be shown that the electric field amplitude at a location x within layer j can be calculated as

$$E_j(x) = (D_{j11}/S_{j11}e^{-i\beta_j(d_j-x)} + D_{j21}/S_{j11}e^{i\beta_j(d_j-x)})E_0^+. \quad (8)$$

2.2. Raman signal generation: discontinuity in Raman active layer and coherency consideration

In general, the Raman signal generated at location x is proportional to the optical field intensity I_{opt} of the incident laser, with units of W/m^2 . It can be determined from the electric field amplitude as

$$I_{opt}(x) = \frac{c\varepsilon_0 n}{2} |E(x)|^2, \quad (9)$$

where c is the speed of light, ε_0 is the permittivity of free space, and n is the material refractive index. Therefore, the Raman signal generated at each location is proportional to the electric field intensity of the incident laser at that location. Referring to Fig. 1, a Raman signal generated at location x is assumed to have the form of a plane wave emanating in both directions with amplitudes E_1 and E_2 in the backward and forward directions, respectively.

Different from the laser propagation evaluation, the transfer matrix method cannot be simply applied to the overall film stack to evaluate the Raman signal propagation. Here we first apply the transfer matrix method to the layers before and after the Raman active layer. Then the Raman signal discontinuity is accurately considered in the Raman active layer. As shown in Fig. 1, the generated Raman signal propagating from location x within layer j in the forward and backward directions are considered separately due to their different contributions to the resultant measured intensity. At this point, we take the generated Raman signal propagating in each direction to have unit amplitude and an arbitrary phase shift. For the Raman scattering in the backward direction, E_1 , the resultant electric field amplitude in the layer j just prior to the interface between layers j and $j+1$, we have

$$\begin{bmatrix} E_{j2}^+ \\ E_{j2}^- \end{bmatrix} = D \begin{bmatrix} E_{m+1}^+ \\ 0 \end{bmatrix}. \quad (10)$$

It can be quickly shown that $E_{j2}^-/E_{j2}^+ = D_{21}/D_{11}$. From E_j^+ to E_{j2}^+ , the electric field amplitude varies continuously and we have $E_j^+ = E_{j2}^+ e^{-i\beta_j d_j}$. However, from E_{j2}^- to E_j^- , due to Raman signal generation (backward) at location x , the electrical field has a unit step change after the light passes this location. Considering this discontinuity, we have

$$E_j^- = E_{j2}^- e^{i\beta_j d_j} + e^{i\beta_j x} = \frac{D_{21}}{D_{11}} E_{j2}^+ e^{i\beta_j d_j} + 1 \times e^{i\beta_j x}. \quad (11)$$

Then the Raman scattering light on the left side of the Raman active layer j can be described as

$$\begin{bmatrix} 0 \\ E_0^- \end{bmatrix} = U \begin{bmatrix} E_j^+ \\ E_j^- \end{bmatrix} = U \begin{bmatrix} E_{j2}^+ e^{-i\beta_j d_j} \\ \frac{D_{21}}{D_{11}} E_{j2}^+ e^{i\beta_j d_j} + e^{i\beta_j x} \end{bmatrix}. \quad (12)$$

From the above equation, we will have

$$0 = U_{11} E_{j2}^+ e^{-i\beta_j d_j} + U_{12} \frac{D_{21}}{D_{11}} E_{j2}^+ e^{i\beta_j d_j} + U_{12} e^{i\beta_j x}. \quad (13)$$

Finally, solving for E_{j2}^+ we have

$$E_{j2,1}^+ = \frac{-U_{12} e^{i\beta_j x}}{U_{11} e^{-i\beta_j d_j} + U_{12} D_{21}/D_{11} \cdot e^{i\beta_j d_j}}, \quad (14)$$

and the backward Raman scattering emitted from the film stack is

$$E_0^-|_{backward} = U_{21}E_{j,2}^+e^{-i\beta_j d_j} + U_{22}[D_{21}/D_{11} \cdot E_{j,2}^+e^{i\beta_j d_j} + e^{i\beta_j x}]. \quad (15)$$

In these equations, U and D are the same transfer matrices from Eq. (6) and Eq. (7), respectively, except calculated using the wavelength of the Raman scattered light and the complex refractive index at that wavelength. A similar approach is taken for the forward scattered Raman light E_2 :

$$E_{j,2}^+ = \frac{U_{11}e^{-i\beta_j x}}{U_{11}e^{-i\beta_j d_j} + U_{12}D_{21}/D_{11} \cdot e^{i\beta_j d_j}}. \quad (16)$$

The contribution to the Raman signal at the surface from the forward scattered light is

$$E_0^-|_{forward} = U_{21}[E_{j,2}^+e^{-i\beta_j d_j} - e^{-i\beta_j x}] + U_{22}D_{21}/D_{11} \cdot E_{j,2}^+e^{i\beta_j d_j}. \quad (17)$$

We rename the backward and forward propagating Raman light emerging from the surface as $E_{0,b}^-$ and $E_{0,f}^-$, respectively. Combining these equations for the case where the forward and backward Raman signals are coherent and emitted with the same phase, we obtain a dimensionless enhancement factor to the Raman signal of $|E_{0,b}^- + E_{0,f}^-|^2$ which can be calculated at each location x in layer j . As noted, the Raman signal generated at each location x is proportional to intensity of the incident light $|E_j(x)|^2$. The total Raman signal measured at the surface of the multi-layer film stack can be found from the integral over the Raman-active layer thickness

$$I_{Raman} = \int_j [|E_j(x)|^2 \cdot |E_0^-|_{backward} + E_0^-|_{forward} |^2] dx. \quad (18)$$

In general, the backward and forward propagating Raman signals may not be in phase. We can introduce an arbitrary phase shift ϕ between them to obtain the total intensity

$$I_{Raman} = \int_j [|E_j(x)|^2 \cdot |E_{0,b}^- + E_{0,f}^- e^{i\phi}|^2] dx, \quad (19)$$

where ϕ is a random phase shift. Expanding the term $|E_{0,b}^- + E_{0,f}^- e^{i\phi}|^2$ and integrating over ϕ will lead to the below expression for the incoherent case:

$$I_{Raman} = \int_j [|E_j(x)|^2 \cdot (|E_{0,b}^-|^2 + |E_{0,f}^-|^2)] dx. \quad (20)$$

3. Results and discussion

This transfer matrix-based methodology for calculating the Raman intensity as a function of layer thickness for multi-layer thin films is applicable to any multi-layer thin film with an arbitrary number of layers. As shown in the following sections, it may be used to predict the Raman intensity as a non-monotonic function of layer thickness. Additionally, in the calculation, the layer which is being varied in thickness need not be the same layer for which the Raman signal is being measured. A MATLAB program was written to perform these calculations. The inputs to the model are the complex index of refraction for each material layer at both the incident wavelength and the Raman scattered wavelength, and the thickness of each layer. Three material systems are evaluated: silicon-on-sapphire, multi-layer graphene on a substrate, and multi-layer MoS₂ where a gap exists between film and substrate.

3.1. Silicon-on-sapphire: three periodical variations of Raman intensity

Epitaxial silicon grown on sapphire substrates, known as silicon-on-sapphire (SOS), is used to fabricate electronic circuits with a small footprint and lower energy consumption [26]. These benefits are a consequence of the highly insulating sapphire substrate, which has a low parasitic capacitance. Due to the slight mismatch in the atomic spacing between the sapphire R-plane and the Si 100 plane, significant residual stresses can develop [27]. Raman spectroscopy is one tool that can be used to probe these stresses. However, the intensity of the Raman signal will vary non-monotonically with the thickness of the Si film due to interference of the incident and Raman scattered light. Here, the intensity of the 521 cm^{-1} Raman shift is calculated as a function of Si film thickness. The wavelength of the excitation light is 532 nm. The indices of refraction used in the calculation are $4.152 + 0.052i$ and $4.096 + 0.043i$ for Si at the excitation and wavelengths, respectively [28]. For the sapphire substrate, the corresponding indices of refraction are 1.772 and 1.770 [29]. In Fig. 2(a), the Raman intensity is calculated for the cases where the forward and backward Raman scattering are coherent [Eq. (18)] and incoherent [Eq. (21)]. An enlargement of the Raman intensity for Si thicknesses up to 500 nm is shown in the inset of Fig. 2(a). It is clear that the Raman intensity for the coherent case is larger than the incoherent case. This is to be expected; in the superposition of incoherent waves, there will be more negative interference leading to a lower amplitude. The ratio between the coherent signal to the incoherent signal is given in the inset of Fig. 2(b). As the Si thickness increases, the coherent intensity converges with the incoherent intensity as more of the reflected signal is absorbed.

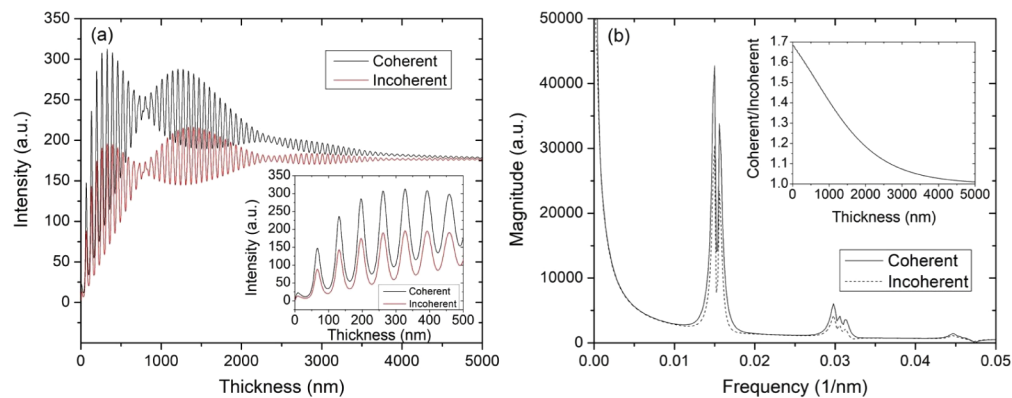


Fig. 2. Calculated intensity of the 521 cm^{-1} Si Raman shift as a function of Si film thickness on a sapphire substrate. (a) The non-monotonic variation in the Raman intensity vs. thickness is due to interference of both incident and Raman scattered light calculated for the cases of coherent and incoherent combination. The secondary lower frequency variation in Raman intensity is due to difference in wavelength between incident and Raman scattered light. Inset: An enlargement of the variation in Raman intensity for Si film thickness up to 500 nm. (b) FFT of calculated Raman intensity vs thickness curve. Two frequencies are found. The first, with period 64.1 nm corresponds to interference of the incident light. The second, with period 66.7 nm corresponds to interference of the Raman scattered light. Inset: ratio of intensity from the coherent case to intensity from incoherent case.

In Fig. 2(a) the periodic variation of the intensity of the Raman scattered signal is apparent. This is a result of multiple reflections of both the incident and Raman scattered light at the thin film interfaces creating interference. It is also noted in Fig. 2(a) that there appears to be a secondary, lower frequency in the variation of Raman signal intensity with thickness. Referring to Eq. (20), the contribution to the Raman intensity from a location x within the Si film is the electric field amplitude of the Raman light at the surface calculated by the TMM. This is weighted

by the amplitude of the incident light at location x [Eq. (9)]. There is a small difference in the wavelength of the incident light (532 nm) and the Raman scattered light (521 cm^{-1}). Due to this difference in wavelength, the two terms in Eq. (20) will have slightly different frequencies. A fast Fourier transform (FFT) was performed on the data in Fig. 2(a) and two frequencies were identified [Fig. 2(b)]. The FFT was performed on the data from both the coherent and incoherent cases. The same two frequencies were identified in both cases. The first, with a period of 64.1 nm, corresponds to interference of the incident light. The second, with a period of 66.7 nm, corresponds to the interference of the Raman scattered light. This results in a secondary variation with a period of around 1667 nm, which corresponds to the observed variation in Fig. 2.

In general, the interference of the incident light and the Raman scattered light will have separate impacts on the measured Raman intensity as a function of film thickness. For normally incident laser light, the optical field intensity within the film of interest will have a periodic variation in the thickness direction with a period given by $T_{inc} = \lambda_{inc}/2n$. The factor “2” comes from the fact after reflected from the bottom interface, the light will travel a distance of double film thickness to constructively interfere with the light reflected at the top interface. Similarly, constructive interference of the Raman scattered light emerging from the film varies with the film thickness with a period given by $T_{Raman} = \lambda_{Raman}/2n$. Based on these equations, the periods are calculated to be $T_{inc} = 64.07 \text{ nm}$ and $T_{Raman} = 66.79 \text{ nm}$, which agree very well with the periods uncovered by Fig. 2(b): 64.1 nm and 66.7 nm. The superposition of these trends results in the observed variation in Raman intensity vs thickness, with a period $\omega = 2(1/T_{inc} + 1/T_{Raman})^{-1}$. The larger, secondary variation can be found as $\omega_s = (1/T_{inc} - 1/T_{Raman})^{-1}$. This gives a period of 1573 nm, which is exactly found in the simulation data. These equations can be quickly used to estimate the period in the variation of measured Raman intensity as a function of thin film thickness.

3.2. Multi-layer graphene and comparison with reported work

It has previously been noted that the Raman signal from multi-layer graphene on Si substrates can be enhanced with a SiO_2 capping layer [20,21]. This signal enhancement is due the interference effects from multiple reflections of the incident and Raman scattered light within the thin film layers. Previous studies have calculated this effect from the Fresnel equations. Here, the Raman signal intensity is calculated using the described method. The complex indices of refraction used in the calculation are experimentally determined values from the literature and are given in Table 1. A single value for the graphene index of refraction is used as a first approximation. Here, incoherent combination of the forward and backward scattered Raman signal is assumed [Eq. (20)].

Table 1. Optical Constants Used in Graphene Raman Intensity Calculation

Material	Incident (532 nm)	Raman G-band (1586 cm^{-1})	Ref.
Graphene	$2.679 + 1.223i$	$2.685 + 1.287i$	[30]
SiO_2	$1.467 + 0.002i$	$1.465 + 0.002i$	[31]
Si	$4.152 + 0.052i$	$3.995 + 0.037i$	[28]

In Fig. 3(a), the Raman intensity is calculated for varying multi-layer graphene thicknesses; from 1 to 50 layers, with a fixed SiO_2 layer thickness of 100 nm. The incident laser light is 532 nm, and the intensity is calculated for the graphene G-band (1586 cm^{-1}). The thickness of an individual graphene layer is taken to be 0.34 nm. As the thickness of the multi-layer graphene increases, the Raman intensity increases until about 17 layers, then decreases roughly linearly with number of layers. This is due to the increasing absorption of the incident light as the number of layers increases. In Fig. 3(b), the intensity of the graphene G-band is calculated for single-layer graphene on a Si substrate with an SiO_2 layer that varies from 0–500 nm. Because this is not a simple film on a substrate and the layer that is varying in thickness is not the same as the Raman

active layer, the period of the variation in Raman intensity with film thickness cannot be simply calculated as above. However, because the graphene layer is thin compared to the SiO₂ layer, using the index of refraction for SiO₂ provides a good estimate. For example, the period in the Raman intensity against thickness curve is estimated using the index of refraction of SiO₂ as 189.4 nm, while the actual period shown in Fig. 3(b) is 187 nm.

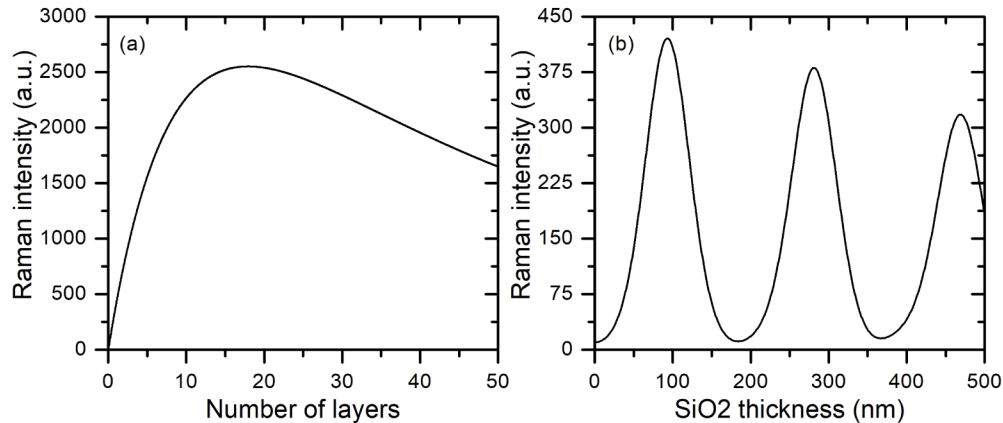


Fig. 3. Interference effects on intensity of 1586 cm^{-1} graphene Raman shift (G-band), using 532 nm excitation. (a) Intensity of multi-layer graphene G-band Raman signal with increasing number of layers, for a 100 nm SiO₂ layer. (b) Intensity of G-band Raman shift from a single-layer graphene for increasing SiO₂ layer thickness.

In Fig. 4, the calculated intensity of the graphene G-band Raman shift from single-layer graphene as a function of SiO₂ thickness is calculated and compared to that calculated in [21]. In this case, the excitation light had a wavelength of 514.5 nm. In [21], the calculation of the Raman intensity was done with the approximation that Raman scattered light was at the same wavelength as the incident light, and also using the actual wavelength of the Raman scattered light, and a significant deviation was noted between the two. Also, in [21], the backward and forward Raman generation are assumed to have zero phase shift at emission. The improved calculation of the Raman intensity using the TMM follows a similar trend as the previous work, with a pronounced difference at larger thicknesses. The period of the variation of the Raman intensity with SiO₂ thickness of the present calculation falls between that of the two cases in [21]. This is because in the previous work, either interference of the incident light or the Raman scattered light was considered, but the compound effects of both were not properly considered. This also accounts for the smaller magnitude at large thicknesses; a secondary variation would be apparent if the calculation was extended to larger SiO₂ thicknesses.

3.3. Effect of interface spacing and layer number for multi-layered TMDs

The final material system to be evaluated is multilayer MoS₂ on a Si substrate. Mechanically exfoliated MoS₂ layers which are transferred to a substrate can have significant corrugations and imperfect interfaces with the substrate. This can have significant impact on the energy coupling and transport between the MoS₂ layers and the substrate. Probing of the energy transport properties by Raman spectroscopy of these can be significantly affected by the presence of gaps or spacing between the TMD layer and substrate [32].

In Fig. 5, the intensity of the E_{2g}^1 Raman shift (383 cm^{-1}) is calculated for several MoS₂ layers (1–10) and a range of gap spacings between the layers and the Si substrate (0–5 nm), assuming incoherent combination of the backward and forward scattered Raman light. Again, the excitation light is assumed to have a wavelength of 532 nm. The thickness of an individual

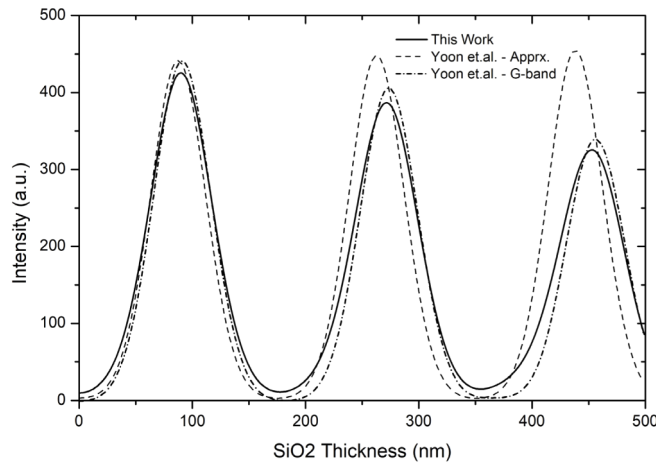


Fig. 4. Calculated intensities of the Raman G-band of single-layer graphene as a function of SiO₂ layer thickness. Calculated Raman intensity based on the TMM approach is compared to those calculated in [21].

layer of MoS₂ was taken to be 0.72 nm. The complex index of refraction of bulk MoS₂ was used in the calculation ($5.238 + 1.160i$ for incident light, $5.131 + 1.129i$ for Raman scattered light) [33]. From Fig. 5(a) it is seen that the Raman intensity increases with MoS₂ thickness for the first ten layers, but that the rate of increase is larger for larger gap spacings. The presence of a gap between the MoS₂ and Si substrate provides some enhancement of the Raman signal. The relative Raman intensity compared to no gap is shown in Fig. 5(b). This enhancement appears minimal for small numbers of layers, but becomes more significant at larger numbers of layers. For example, the enhancement of the Raman signal with a 5 nm gap spacing is only around 14% compared to no gap spacing for an MoS₂ monolayer, but increases to a 37% enhancement for 10 layers.

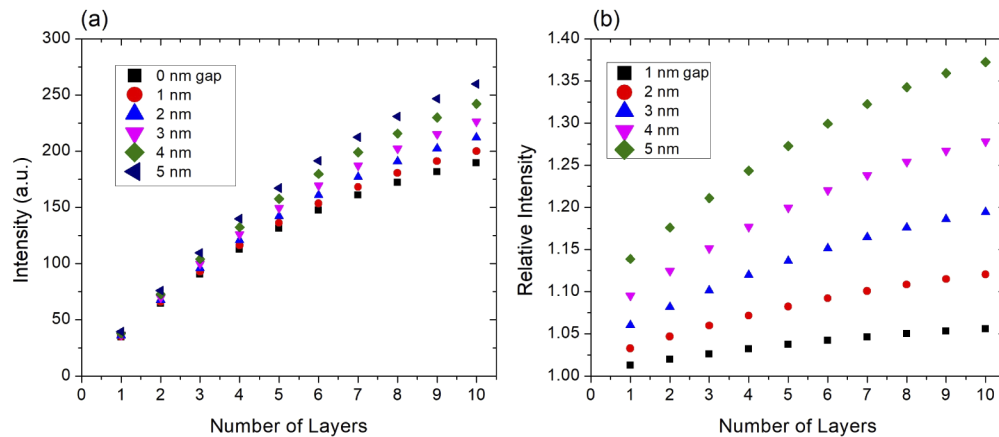


Fig. 5. (a) Calculated intensity of the E_{2g}^1 Raman shift of multilayer MoS₂ on Si with a gap between the layers and substrate. The rate of increase in intensity with number of layers increases with the gap spacing, illustrating the signal enhancement effect due to interference that results from the presence of the gap. (b) Relative Raman intensity due to gap spacing between MoS₂ layers and substrate.

3.4. Discussions

The transfer matrix approach to predicting the Raman signal intensity from multilayer thin film stacks has a number of potential applications for probing physical properties and interpreting experimental data. This approach calculates the Raman intensity as a function of layer thickness, which provides an opportunity for metrology of multilayer thin films, where other thickness measurement techniques may not be sufficient. For example, in the case of silicon-on-sapphire thin films illustrated previously, measuring the thickness of SOS film using traditional ellipsometry is challenging due to the optical properties of the sapphire substrate. Additionally, the technique may prove useful for simultaneous measurement of the thickness of multiple distinct, Raman-active layers within a multi-layer film stack. Alternatively, the inverse problem can be addressed. By measuring the Raman spectra of multiple thin film samples with known thicknesses, the transfer matrix approach could provide a means for an alternative determination of the complex index of refraction. This may be particularly advantageous for two dimensional materials such as graphene and TMDs.

Another application for this Raman intensity calculation is in the fabrication of samples for the Raman probing of 2D materials such as graphene and TMDs. Substrates that 2D material samples are deposited on can be optimized to maximize the enhancement of the Raman signal when probing the properties of these materials with Raman spectroscopy. For example, the thickness of the SiO₂ layer on a Si substrate to which graphene is deposited can be optimized to maximize the Raman signal from the graphene layer. Similarly, the layers of Van der Waals heterostructures constructed from 2D materials can be probed and optimized to enhance the Raman spectra of interest. Finally, when corrugation or other separation of layers and substrate may be expected, the TMM approach to predicting Raman signal intensity can provide insight into the quality of the interface between 2D material and substrate.

Note that in the practical application of Raman spectroscopy, there are many instrument parameters that impact the measured signal intensity, from laser power to detector quantum efficiency. For this reason, Raman intensities are typically reported in arbitrary units (a.u.). In the practical application of the TMM-based calculation of the Raman signal intensity from multi-layer thin films, an instrument-specific scaling factor should be applied to the values calculated in Eq. (18) and Eq. (20), assuming that instrument parameters are maintained through repeated measurements.

4. Conclusion

In this study, a method for calculating the intensity of a Raman signal from a thin film within a multilayer thin film stack with an arbitrary number of layers with arbitrary thicknesses was developed based on the transfer matrix method. The discontinuity of the Raman light within the Raman active layer was considered rigorously. Also, both coherent and incoherent forward and backward Raman scattering were considered. This technique was applied to several different thin film material systems to demonstrate the versatility of the developed approach. This includes silicon-on-sapphire thin films. Interference effects from both the incident light and the Raman scattered light impact the calculation of the Raman signal as a function of film thickness. Three frequencies were observed in the Raman signal variation against film thickness, reflecting the interference of the incident light, Raman signal, and their differential. Other applications include Raman probing of two-dimensional material such as graphene and TMDs like MoS₂. The enhancements of the Raman signal due to the thickness of underlying layers or gaps between film layers and substrate were calculated. Several applications for this calculation are contemplated for future experimental validation.

Funding

National Science Foundation (CBET1930866); Defense Microelectronics Activity (HQ072718C0008).

Disclosures

The authors declare no conflicts of interest.

References

1. A. H. Atabaki, S. Moazeni, F. Pavanello, H. Gevorgyan, J. Notaros, L. Alloatti, M. T. Wade, C. Sun, S. A. Kruger, H. Meng, K. Al Qubaisi, I. Wang, B. Zhang, A. Khilo, C. V. Baiocco, M. A. Popovic, V. M. Stojanovic, and R. J. Ram, "Integrating photonics with silicon nanoelectronics for the next generation of systems on a chip," *Nature* **556**(7701), 349–354 (2018).
2. R. A. Street, "Thin-Film Transistors," *Adv. Mater.* **21**(20), 2007–2022 (2009).
3. M. Eslamian, "Inorganic and organic solution-processes thin film devices," *Nano-Micro Lett.* **9**(1), 3 (2017).
4. R. Venkatasubramanian, E. Siivola, T. Colpitts, and B. O'Quinn, "Thin-film thermoelectric devices with high room-temperature figures of merit," *Nature* **413**(6856), 597–602 (2001).
5. J.-H. Kim, W.-J. Kim, and T.-S. Oh, "Thermoelectric thin film devices for energy harvesting with the heat dissipated from high-power light-emitting diodes," *J. Electron. Mater.* **45**(7), 3410–3417 (2016).
6. A. A. Balandin, S. Ghosh, W. Bao, I. Calizo, D. Teweldebrhan, and C. N. Lau, "Superior thermal conductivity of single-layer graphene," *Nano Lett.* **8**(3), 902–907 (2008).
7. H. Sun, Z. Xu, and C. Gao, "Multifunctional, ultra-flyweight, synergistically assembled carbon aerogels," *Adv. Mater.* **25**(18), 2554–2560 (2013).
8. Q. H. Wang, K. Kalantar-Zadah, A. Kis, J. N. Coleman, and M. S. Strano, "Electronics and optoelectronics of two-dimensional transition metal dichalcogenides," *Nat. Nanotechnol.* **7**(11), 699–712 (2012).
9. W. Choi, N. Choudhary, G. H. Han, J. Park, D. Akinwande, and Y. H. Lee, "Recent development of two-dimensional transition metal dichalcogenides and their applications," *Mater. Today* **20**(3), 116–130 (2017).
10. H. Lim, S. Yoon, G. Kim, A. Jang, and H. Shin, "Stacking of two-dimensional materials in lateral and vertical directions," *Chem. Mater.* **26**(17), 4891–4903 (2014).
11. K.S. Novoselov, A. Mishchenko, A. Carvalho, and A.H. Castro Neto, "2D materials and van der Waals heterostructures," *Science* **353**(6298), aac9439 (2016).
12. E. Smith and G. Dent, *Modern Raman Spectroscopy: A Practical Approach* (John Wiley and Sons, Inc., 2005).
13. A. Kudelski, "Analytical applications of Raman spectroscopy," *Talanta* **76**(1), 1–8 (2008).
14. L. M. Malard, M. A. Pimenta, G. Dresselhaus, and M. S. Dresselhaus, "Raman spectroscopy in graphene," *Phys. Rep.* **473**(5–6), 51–87 (2009).
15. Y. Yue and X. Wang, "Nanoscale thermal probing," *Nano Rev.* **3**(1), 11586–11596 (2012).
16. Y. Yue, J. Zhang, and X. Wang, "Micro/nanoscale spatial resolution temperature probing for interface thermal characterization between epitaxial graphene and 4H-SiC," *Small* **7**(23), 3324–3333 (2011).
17. P. Yuan, R. Wang, H. Tan, T. Wang, and X. Wang, "Energy Transport State Resolved Raman for Probing Interface Energy Transport and Hot Carrier Diffusion in Few-Layered MoS₂," *ACS Photonics* **4**(12), 3115–3129 (2017).
18. P. Yuan, H. Tan, R. Wang, T. Wang, and X. Wang, "Very fast hot carrier diffusion in unconstrained MoS₂ on glass substrate: discovered by picosecond ET-Raman," *RSC Adv.* **8**(23), 12767–12778 (2018).
19. J. W. Ager III, D. K. Veirs, and G. M. Rosenblatt, "Raman intensities and interference effects for thin films adsorbed on metals," *J. Chem. Phys.* **92**(3), 2067–2076 (1990).
20. Y. Y. Wang, Z. H. Ni, Z. X. Shen, H. M. Wang, and Y. H. Wu, "Interference enhancement of Raman signal of graphene," *Appl. Phys. Lett.* **92**(4), 043121 (2008).
21. D. Yoon, H. Moon, Y.-W. Son, J. S. Choi, B. H. Park, Y. H. Cha, Y. D. Kim, and H. Cheong, "Interference effect on Raman spectrum of graphene on SiO₂/Si," *Phys. Rev. B* **80**(12), 125422 (2009).
22. M. Born and E. Wolf, *Principles of Optics*, 7th Ed. (Cambridge University 1999).
23. C. Katsidis and D. Siapkas, "General transfer-matrix method for optical multilayer systems with coherent, partially coherent, and incoherent interference," *Appl. Opt.* **41**(19), 3978–3987 (2002).
24. M. C. Tropicovsky, A. S. Sabau, A. R. Lupini, and Z. Zhang, "Transfer-matrix formalism for the calculation of optical response in multilayer systems: from coherent to incoherent interference," *Opt. Express* **18**(24), 24715–24721 (2010).
25. P. Peumans, A. Yakimov, and S. Forrest, "Small molecular weight organic thin-film photodetectors and solar cells," *J. Appl. Phys.* **93**(7), 3693–3723 (2003).
26. T. Nakamura, H. Matsuhashi, and Y. Nagatomo, "Silicon on Sapphire (SOS) Device Technology," *Oki Tech. Rev.* **71**(200), XII–XIII (2004).
27. A. Pramanik and L. C. Zhang, "Residual stresses in silicon-on-sapphire thin film systems," *Int. J. Solids Struct.* **48**(9), 1290–1300 (2011).
28. D. E. Aspnes and A. A. Studna, "Dielectric functions and optical parameters of Si, Ge, GaP, GaAs, GaSb, InP, InAs, and InSb from 1.5 to 6.0 eV," *Phys. Rev. B* **27**(2), 985–1009 (1983).
29. I. Malitson, "Refraction and dispersion of synthetic sapphire," *J. Opt. Soc. Am.* **52**(12), 1377–1379 (1962).

30. J. W. Weber, V. E. Calado, and M. C. M. van de Sandan, "Optical constants of graphene measured by spectroscopic ellipsometry," *Appl. Phys. Lett.* **97**(9), 091904 (2010).
31. L. Marcos, J. Larruquert, J. Mendez, and J. Aznarez, "Self-consistent optical constants of SiO₂ and Ta₂O₅ films," *Opt. Mater. Express* **6**(11), 3622–3657 (2016).
32. P. Yuan, C. Li, S. Xu, J. Liu, and X. Wang, "Interfacial thermal conductance between few to tens of layered-MoS₂ and c-Si: Effect of MoS₂ thickness," *Acta Mater.* **122**, 152–165 (2017).
33. A. R. Beal and H. P. Hughes, "Kramers-Kronig analysis of the reflectivity spectra of 2H-MoS₂, 2H-MoSe₂ and 2H-MoTe₂," *J. Phys. C: Solid State Phys.* **12**(5), 881–890 (1979).